GRZEGORZ STORY*, MARIAN KORDAS*, RAFAŁ RAKOCZY*

ANALYSIS OF A MIXING PROCESS INDUCED BY A ROTATING MAGNETIC FIELD BY MEANS OF THE DIMENSIONAL ANALYSIS

ANALIZA PROCESU MIESZANIA INDUKOWANEGO PRZEZ WIRUJĄCE POLE MAGNETYCZNE ZA POMOCĄ ANALIZY WYMIAROWEJ

Abstract

The main objective of this work is to study the effect of rotating magnetic field (RMF) on the hydrodynamic conditions in the mixed liquid. The dimensional analysis of Navier-Stokes equations including the Lorenz force allows describing the analyzed process by using the relationships basing on the dimensionless numbers. The comparison between the obtained results and the experimental investigations is carried out. It was found a strong correlation between the velocity field and the magnetic induction or electrical conductivity of fluid.

Keywords: *mixing process*, *magnetic field*, *dimensionless numbers*

Streszczenie

Głównym celem pracy było zbadanie wpływu wirującego pola magnetycznego na warunki hydrodynamiczne panujące mieszalniku. Przeprowadzono analizę wymiarową równania Naviera-Stokesa, włączając siły Lorenza. Na podstawie wyprowadzonych zależności wyznaczono obwodową prędkość cieczy poddanej wpływom wirującego pola magnetycznego. Uzyskane wartości potwierdzono doświadczalnie. Wyniki przedstawiono w postaci map prędkości. Stwierdzono silną zależność pomiędzy wartościami prędkości a indukcją magnetyczną i przewodnością elektryczną płynu

Słowa kluczowe: *mieszanie*, *pole magnetyczne*, *bezwymiarowe liczby*

* M.Sc. Grzegorz Story, Ph.D. Eng. Marian Kordas, D.Sc. Ph.D. Eng. Rafał Rakoczy, Institute of Chemical Engineering and Environmental Protection Process, West Pomeranian University of Technology, Szczecin.

1. Introduction

The design, scale-up and optimization of industrial processes conducted in agitated systems require, among other, precise knowledge of the hydrodynamics, mass and heat transfer parameters and reaction kinetics. One of the key aspects in the dynamic behavior of the mass-transfer and heat-transfer processes is the role of hydrodynamics. On a macroscopic scale, the improvement of hydrodynamic conditions can be achieved by using various techniques of mixing, vibration, rotation, pulsation and oscillation in addition to other techniques like the use of fluidization, turbulence promotes or magnetic and electric fields etc.

One of the parameters characterizing the mixing process is the mixing efficiency. This parameter determines the amount of energy which is needed to achieve intended technological objective. The rotating magnetic field (RMF) is a versatile option for enhancing several physical and chemical processes. Studies over the recent decades were focused on application of magnetic field (MF) in different areas of chemical engineering and biotechnology [1]. Static, rotating or alternating MFs might be used to augment the process intensity instead of mechanically mixing. The practical applications of MFs are presented in the relevant literature [2–7].

Recently, TRMF are widely used to control different processes in the various engineering operations [8–12]. This kind of magnetic field induces a time-averaged azimuthal force, which drives the flow of the electrical conducting fluid in circumferential direction. According to available in technical literature, the mass-transfer during the solid dissolution to the surrounding liquid under the action of TRMF has been deliberated [13, 14].

The mixing process of liquids is often realized in the mixing tank or stirred vessel. The efficiency of the mixing process is assessed by means of the mechanical characteristics such as power consumption of agitator or mixing time. Static or rotating magnetic field might be used to augment the process intensity instead of mechanical mixing. One of advantages of the RMF is the possibility to apply them to generation and control of the hydrodynamic states for the magnetic particle disperse systems.

The objective of this study is to evaluate the hydrodynamic conditions in the mixing process that is induced under the action of the RMF. It is decided that in the present report, the influence of the RMF on the mixing process is described by using the non-dimensional parameters formulated on the base of fluid mechanics equations. Based on these relations, the fluid velocity under the action of the RMF was determined.

2. Theoretical background

The interaction of the applied magnetic field with the liquid may be described by means of the Navier-Stokes equation of motion. The flow under the action of the RMF may be determined by including the Lorentz force to this relation. The non-dimensional for of the above equation may be presented in the following form [15]:

$$S^{-1}\left[\frac{\partial \rho_p^* w_p^*}{\partial \tau^*}\right] + [div^*(\rho_p^* w_p^* w_p^*)] = Fr^{-1}[\rho_p^* F^*] - Eu^{-1}[grad^* \, p^*] + Re^{-1}[\eta_p^* \Delta^* w_p^*] +$$

$$+ Re^{-1}\left[2\eta_{rot_p}^* rot^*\left(\frac{1}{2} rot^* w_p^*\right)\right] + Eu_{e,q}[\rho_p^* E^*] + \tag{1}$$

$$- 2\,Re_e\,Eu_m[\sigma_e^* \mu_m^* (E^* \times H^*)] - Ta_m\,Re^{-2}[\sigma_e^*(\mu_m^*)^2(w^* \times H^*) \times H^*]$$

where:

E	–	electric field intensity [mkgA^{-1}s^{-3}],
F	–	force [N],
H	–	magnetic field intensity [A m^{-1}],
p	–	hydrostatic pressure [Pa],
w	–	velocity [ms^{-1}],
w_p	–	fluid velocity [ms^{-1}],
η_p	–	dynamic viscosity coefficient of fluid [Pas],
η_{rot_p}	–	dynamic rotational viscosity coefficient of fluid [Pas],
μ_m	–	magnetic permeability [kgmA^{-2}s^{-2}],
ρ_p	–	fluid density [kgm^{-3}],
σ_e	–	conductivity [A^{2}s^{3}kg^{-1}m^{-3}],
τ	–	time [s].

The above equation (1) includes the non-dimensional group characterizing the mixing problem, namely:

Strouhal's number
$$S = \frac{w_{p0}\tau_0}{l_0} \tag{2a}$$

Froude's number
$$Fr = \frac{w_{p0}^2}{gl_0} \tag{2b}$$

Euler's number
$$Eu = \frac{p_0}{\rho_{p0} w_{p0}^2} \tag{2c}$$

Reynolds number
$$Re = \frac{w_{p0}l_0}{v_{p0}} \tag{2d}$$

magnetic Euler's number
$$Eu_m = \frac{\mu_{m_{p0}} H_0^2}{2\rho_{p0} w_{p0}^2} \tag{2e}$$

electric Euler's number
$$Eu_e = \frac{\varepsilon_{e_{p0}} E_0^2}{2\rho_{p0} w_{p0}^2} \tag{2f}$$

electric Euler's number
$$Eu_{e,q} = \frac{\rho_{q0} E_0 l_0}{\rho_{p0} w_0^2} \tag{2g}$$

electric Reynolds number

$$\mathrm{Re}_e = \frac{E_0 l_0 \sigma_{e_0}}{H_0} \tag{2h}$$

magnetic Taylor's number

$$\mathrm{Ta}_m = \frac{w_0 l_0^3 B_0^2 \sigma_{e_0}}{\rho_0 \nu_0^2} \tag{2i}$$

where:

l – linear dimension [m],
B_0 – axial magnetic field induction [T],
g – gravity acceleration [ms^{-2}],
ν_p – kinematic viscosity coefficient of fluid [m^{2}s^{-1}],
ε_e – electric permeability [A^{2}s^{4}kg^{-1}m^{-3}].

The above equation (1) also determines the following relationships

$$\mathrm{Eu}_m \propto \mathrm{Re}^{-1} \Rightarrow \frac{\mu_{m_{p0}} H_{p0}^2}{2\rho_{p0} w_{p0}^2} \propto \frac{\eta_{p0}}{l_0 \rho_{p0} w_{p0}} \Rightarrow w_{p0} \propto \frac{\mu_{m_{p0}} H_{p0}^2 l_0}{2\eta_{p0}} \quad \left[\frac{\mathrm{m}}{\mathrm{s}}\right] \tag{3a}$$

$$\mathrm{Eu}_e \propto \mathrm{Re}^{-1} \Rightarrow \frac{\varepsilon_{m_{p0}} E_{p0}^2}{\rho_{p0} w_{p0}^2} \propto \frac{\eta_{p0}}{l_0 \rho_{p0} w_{p0}} \Rightarrow w_{p0} \propto \frac{\varepsilon_{m_{p0}} E_{p0}^2 l_0}{2\eta_{p0}} \quad \left[\frac{\mathrm{m}}{\mathrm{s}}\right] \tag{3b}$$

$$\mathrm{Eu}_{e,q} \propto \mathrm{Re}^{-1} \Rightarrow \frac{\rho_{q0} E_0 l_0}{\rho_{p0} w_{p0}^2} \propto \frac{\eta_{p0}}{l_0 \rho_{p0} w_{p0}} \Rightarrow w_{p0} \propto \frac{\rho_{q0} E_{p0}^2 l_0^2}{\eta_{p0}} \quad \left[\frac{\mathrm{m}}{\mathrm{s}}\right] \tag{3c}$$

where the velocity, w_{p0}, may be interpreted as the liquid velocity under the action of the RMF.

The alternative form of equation which determines the fluid velocity induced by RMF formulated on the basis of $\mathrm{Re}_e \mathrm{Eu}_m$ complex is:

$$\mathrm{Re}_e \, \mathrm{Eu}_m \propto 1 \Rightarrow \frac{\sigma_{e_{p,0}} \mu_{m_{p,0}} E_0 H_0 l_0}{\rho_{p0} w_{p0}^2} \propto 1 \Rightarrow w_{p0} \propto \sqrt{\frac{\sigma_{e_{p,0}} \mu_{m_{p,0}} E_0 H_0 l_0}{\rho_{p0}}} \quad \left[\frac{\mathrm{m}}{\mathrm{s}}\right] \tag{4}$$

It should be noticed that the liquid velocity may be defined as follows:

$$\mathrm{Ta}_m \, \mathrm{Re}^{-2} \propto 1 \Rightarrow \frac{\sigma_{e_{p,0}} \mu_{m_{p,0}}^2 w_{p0} H_0^2 l_0}{\rho_{p0} w_{p0}^2} \propto 1 \Rightarrow \sigma_{e_{p,0}} w_{p0} B_0^2 l_0 \propto \rho_{p0} w_{p0}^2 \tag{5}$$

In the equation (5) replacing the characteristic velocity of the fluid by the maximum peripheral velocity $(w_{p0}^2 \equiv ([w_\varphi]_{\mathrm{max}})^2)$, and expressing the velocity of the fluid by the product of the angular velocity of RMF and linear dimension $(w_{p0} = \omega_{\mathrm{WPM}} l_0)$, we obtained the equation which defines the maximum velocity of fluid:

$$[w_\varphi]_{\mathrm{max}} \propto B_0 l_0 \sqrt{\frac{\sigma_{e_{p,0}} \omega_{\mathrm{RTM}}}{\rho_{p0}}} \quad \left[\frac{\mathrm{m}}{\mathrm{s}}\right] \tag{6}$$

where:

ω_{RTM} – angular velocity of rotating magnetic field [rad s^{-1}].

The above equation (6) may be expressed as follows:

$$w_{\varphi}(f^*, \sigma_e, \rho, R^*, H^*) = B_p(f^*, \sigma_e, R^*, H^*)R^* \sqrt{\frac{\sigma_e \omega_{\text{RTM}}(f^*)}{\rho}} \quad \left[\frac{\text{m}}{\text{s}}\right] \qquad (7)$$

where:

f – frequency of power supply [s^{-1}],
R – radius [m],
H – height [m],
B_p – tranversal magnetic field induction [T].

3. Experimental details

The experimental investigations were carried out using the apparatus, whose scheme are shown in Figure 1. The RMF was created by the generator of magnetic field (1). As the generator of magnetic field the stator from the squirrel-cage type motor was used. A three--phase alternating current flows by the windings of the stator. Inside the generator was a glass container (2), which is filled with the test fluid. Measurements of the magnetic induction were carried out using the magnetic field sensor Asonic SMS-102 – 3 type, which was connected to the computer. The measurements points were located in a container, along the height of the active part of the windings of magnetic field generator and along the radius also.
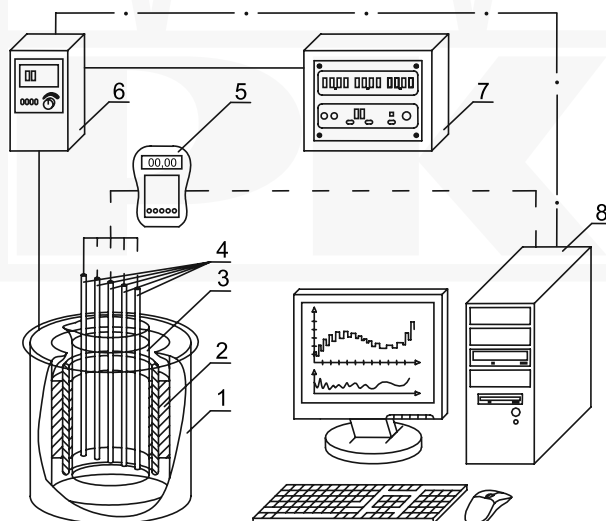

Fig. 1. Experimental apparatus: 1 – cooling jacket, 2 – generator of rotating magnetic field, 3 – glass container, 4 – Hall probes, 5 – magnetic field sensor, 6 – a.c. transistorized inverter, 7 – electronic control box, 8 – personal computer

The scheme of location of the measurements points is shown in Figure 2. This arrangement of measurement points enabled to read the values of the magnetic induction in the whole volume of the mixed liquid. The measurements carried out for the frequency of the generator in the range 1–50 Hz.
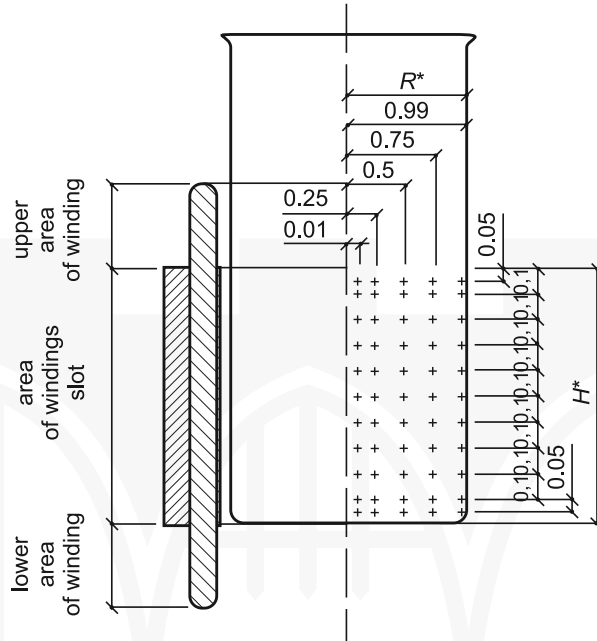

Fig. 2. Distribution measurement points of magnetic induction located on a plane that coincides with the axial section of the stator

It should be noticed that in the present report the tap water (ρ = 998.2 [kg m^{-3}], σ_e = 0.05 [S m^{-1}]), aqueous solution of NaCl 1 wt% (ρ = 1005 [kg m^{-3}], σ_e = 17.6 [S m^{-1}]) and aqueous solution of NaCl 26 wt% (ρ = 1200 [kg m^{-3}], σ_e = 21.56 [S m^{-1}]) were used as the working liquids.

4. Results and discussion

Based on the results of the measurements of magnetic induction in the RMF generator with number of pair poles per phase winding, p, equal to 2, the two-dimensional maps of magnetic induction were plotted. The typical examples of the magnetic induction patterns are shown in Figure 3.

Based on the results of the measurements it was found that magnetic induction at the top and bottom part of the windings was characterized by much lower values than in the central part of the windings, which is called an active part. This is due to dissipation and suppression of the rotating magnetic field. Additionally two-dimensional axial
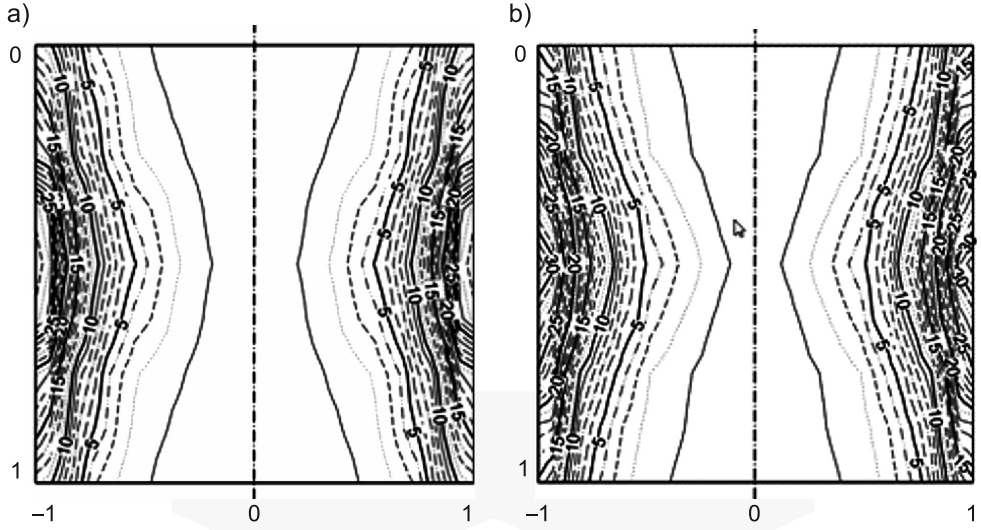
Fig. 3. The spatial distribution of the magnetic field in the cross section of the RMF generator for the frequency: a) $f = 25$ Hz, b) $f = 50$ Hz

symmetry of the distribution magnetic induction was observed, and it allows to simplify the analytical description.

It should be noticed that the obtained form of the equation (7) can be used to determine the analytical description of the liquid velocity fields under the action of the RMF. The magnetic induction is dependent on the operating conditions [15]:

$$B_p(f^*, \sigma_e, R^*, H^*) = \{[B_P]_{\max}(f^*)\} \times$$

$$\times \frac{p_1(f^*, \sigma_e)}{\{1 + [p_2(f^*, \sigma_e)R^* - p_3(f^*, \sigma_e)]^2\}\{1 + [p_4(f^*, \sigma_e)H^* - p_5(f^*, \sigma_e)]^2\}} \quad [\text{mT}] \qquad (8)$$

Substituting equation (8) into equation (7) we have immediately:

$$w_\varphi(f^*, \sigma_e, \rho, R^*, H^*) = \{[B_P]_{\max}(f^*)\}R^* \sqrt{\frac{\sigma_e \omega_{\text{RTM}}(f^*)}{\rho}} \times$$

$$\times \frac{p_1(f^*, \sigma_e)}{\{1 + [p_2(f^*, \sigma_e)R^* - p_3(f^*, \sigma_e)]^2\}\{1 + [p_4(f^*, \sigma_e)H^* - p_5(f^*, \sigma_e)]^2\}} \quad [\text{m} \cdot \text{s}^{-1}] \qquad (9)$$

where the coefficients $p_1(f^*, \sigma_e)$, $p_2(f^*, \sigma_e)$, $p_3(f^*, \sigma_e)$, $p_4(f^*, \sigma_e)$, $p_5(f^*, \sigma_e)$ are given by the following:

$$p_1(f^*,\sigma_e) = 1.1031 + 0.0455\sigma_e - 0.9641f^* - 0.0017\sigma_e^2 + 2.3134f^2$$

$$p_2(f^*,\sigma_e) = 5.5113 + 0.0078\sigma_e - 6.4912f^* - 0.0006\sigma_e^2 + 5.0333f^2$$

$$p_3(f^*,\sigma_e) = 5.9758 + 0.0341\sigma_e - 6,8426f^* - 0.0017\sigma_e^2 + 6.0443f^2 \quad (10)$$

$$p_4(f^*,\sigma_e) = 2,2286 - 0.0051\sigma_e - 1,7925f^* + 0.0001\sigma_e^2 + 2.3483f^2$$

$$p_5(f^*,\sigma_e) = 1.1143 - 0.0026\sigma_e - 0.8962f^* + 6.6202 \times 10^{-5}\sigma_e^2 + 1.2416f^2$$

In the above relationship (9) the parameter $\{[B_P]_{max}(f^*)\}$ is the measured maximal value of the magnetic induction. These values were reported at the point ($R^* = 1$; $H^* = 0.5$) inside the RMF generator.

Figure 4 shows the two-dimensional velocity field patterns. It was observed that the velocity fields are strongly dependent on the electrical conductivity of the fluid and the magnetic induction. Furthermore, the velocity distributions are similar to the distribution of magnetic induction (Fig. 3). It can be concluded that both the fluid velocity and magnetic induction reaches the maximum and minimum values at the same points in the container.

In Figures 5 and 6 the profiles of fluid velocity along the non-dimensional radius and along the dimensionless height of the system are presented. As follows from the analysis of the obtained data, the values of liquid velocity increase with increasing electrical conductivity of the fluid. Based on the Figure 5 it was found that the velocity decreases with
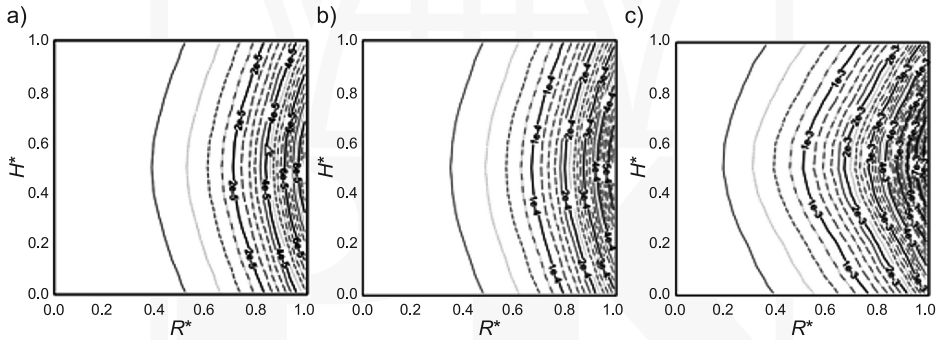

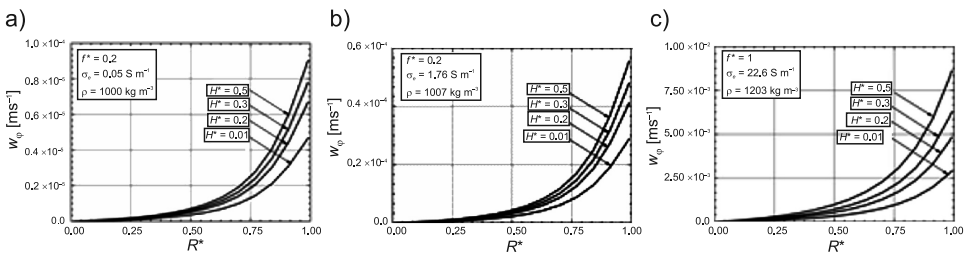Fig. 4. Two-dimensional velocity field for: a) tap water, b) 1 wt% NaCl, c) 26 wt%NaCl

Fig. 5. Velocity profiles along the dimensionless radius at different heights of the system:
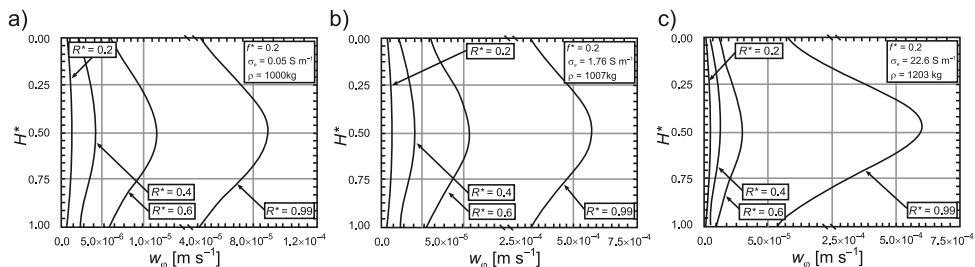a) tap water, b) 1 wt%NaCl, c) 26 wt%NaCl

Fig. 6. Velocity profiles along the dimensionless height for different radial distances:
a) tap water, b) 1 wt% NaCl, c) 26 wt%NaCl

increase distance from the wall of the glass container. In the case of profiles along the height of the beaker (see Fig. 6) velocity of the liquid reached the maximum values at the mid--height of the container. Moreover, these values increase with the increasing distance from the axis of the beaker.

When analyzing the liquid velocity under the action of RMF in the non-uniform magnetic field it is important to determine the representative value of this type of a field. Namely, the averaged value of the liquid velocity may be calculated by integrating the spatial distribution of the liquid velocity. The averaged value of the liquid velocity may be expressed as follows:

$$\left\langle w_\varphi \right\rangle_{\substack{f^*=\text{const},\sigma_e=\text{const} \\ \rho=\text{const}}} = \frac{1}{H^* R^*} \int\limits_{H^*} \int\limits_{R^*} \{w_\varphi(f^*,\sigma_e,\rho,R^*,H^*)\}\, dR^* dH^* \quad [\text{m}\cdot\text{s}^{-1}] \qquad (11)$$

The calculated values of the averaged liquid velocity under the action of the RMF are graphically presented in Fig. 7.
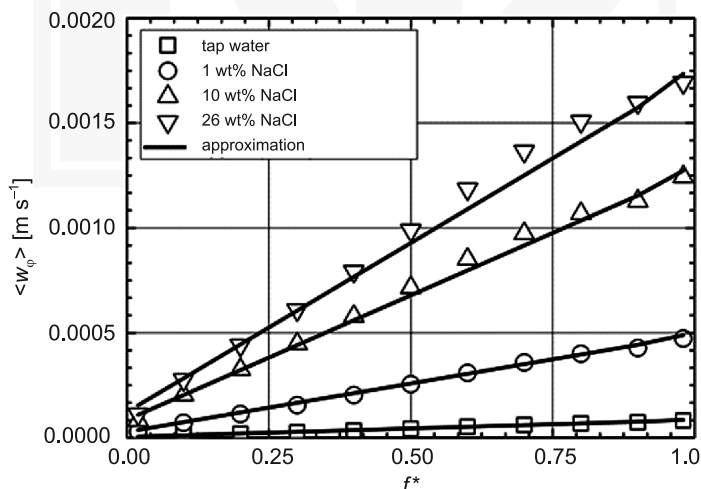

Fig. 7. The typical example of the obtained values of the averaged liquid velocity

The effect of the RMF on the averaged liquid velocity may be described by means of the following relationship:

$$\left\langle w_\varphi(f^*, \sigma_e) \right\rangle = (0.00035\sigma_e^{0.49})f^* + (2 \cdot 10^{-5}\sigma_e^{0.58}) \quad [\text{m} \cdot \text{s}^{-1}] \tag{12}$$

The graph clearly shows that this velocity is not constant for the normalized frequency of the RMF. Fig. 7 demonstrates that, within the scatter limits among the plotted data represented by the points, the averaged liquid velocity increases with increasing the MF intensity.

5. Conclusions

Experimental research and theoretical analysis of the mixing process induced by the rotating magnetic field were performed. An equation to determine the peripheral velocity of the liquid under the influence of a rotating magnetic field was proposed. Based on the results of calculations it was found that:
– there is a strong correlation between the distribution of the velocity field and the magnetic induction or electrical conductivity of fluid,
– the obtained velocity field are qualitatively similar to the distribution of the magnetic induction,
– the highest velocities occur in the middle-height of the generator of rotating magnetic field at the wall and decreases radially and axially with increase the distance from the wall,
– in the axis of the rotating magnetic field generator the value of velocity was close to 0.

References

[1] Hirano M., Ohta A., Abe K., *Magnetic Field Effects on Photosynthesis and Growth of the Cyanobacterium Spirulina platensis*, Journal of Fermentation and Bioengineering, vol. 86(3), 1998, 313-316.

[2] Abbasov T., *Magnetic filtration with magnetized granular beds: Basic principles and filter performance*, China Particuology, vol. 5, 2007, 71-83.

[3] Alvaro A., Rodríguez J.M., Augusto P.A., Estévez A.M., *Magnetic filtration of an iron oxide aerosol by means of magnetizable grates*, China Particuology, vol. 5, 2007, 140-144.

[4] Chen H., Li X., *Effect of static magnetic field on synthesis of polyhydroxyalkanoates from different short-chain fatty acids by activated sludge*, Bioresource Technology, vol. 99, 2008, 5538-5544.

[5] Bau H.H., Zhong J., Yi M., *A minute magneto hydro dynamic (MHD) mixer*, Sensors and Actuators B, vol. 79, 2001, 207-215.

[6] Reichert C., Hoell W.H., Franzreb M., *Mass transfer enhancement in stirred suspensions of magnetic particles by the use of alternating magnetic fields*, Powder Technology, vol. 145, 2004, 131-138.

[7] Chou C., Ho C., Huang C., *The optimum conditions for comminution of magnetic particles driven by a rotating magnetic field using the Taguchi method*, Advanced Powder Technology, vol. 20, 2009, 55-61.

[8] Gelfgat Y., *Electromagnetic filed application in the processes of single crystal growth under microgravity*, Acta Astronautica, vol. 37, 1995, 333-345.

[9] Barmin I.V., Senchenkov A.S., Avetisov I.Ch., Zharikov E.V., *Low-energy methods of mass transfer control at crystal growth*, Journal of Crystal Growth, vol. 275, 2005, e1487-e1493.

[10] Gelfgat Y., *Rotating magnetic fields as a means to control the hydrodynamics and heat/mass transfer in the processes of bulk single crystal growth*, Journal of Crystal Growth, vol. 189/199, 1999, 165-169.

[11] Bellmann M.P., Pätzold O., Gärtner G., Möller H.J., Stelter M., *Radial segregation in VGF-RMF grown germanium*, Journal of Crystal Growth, vol. 311, 2009, 1471-1474.

[12] Yang M., Ma N., Bliss D.F., Bryant G.G., *Melt motion during liquid-encapsulated Czochralski crystal growth in steady and rotating magnetic fields*, International Journal of Heat and Fluid Flow, vol. 28, 2007, 768-776.

[13] Rakoczy R., *Enhancement of solid dissolution process under the influence of rotating magnetic field*, Chemical Engineering and Processing, vol. 49, 2010, 42-50.

[14] Rakoczy R., Masiuk S., *Influence of Transverse Rotating Magnetic Field on Enhancement of Solid Dissolution Process*, American Institute of Chemical Engineers, vol. 56(6), 2010 1416-1433.

[15] Rakoczy R., *Analiza teoretyczno-doświadczalna wpływu wirującego pola magnetycznego na wybrane operacje i procesy inżynierii chemicznej*, Wydawnictwo Uczelniane ZUT, Szczecin 2011.